Wu, J.R., Di Sarno, L., Freddi, F., D'Aniello, M (2022). Modelling of Masonry Infills in Existing Steel Moment-Resisting Frames: Nonlinear Force-Displacement Behaviour. Engineering Structures, 267: 114699. https://doi.org/10.1016/j.engstruct.2022.114699

Modelling of Masonry Infills in Existing Steel Moment-Resisting Frames: Nonlinear Force-Displacement Relationship

Jing-Ren Wu[1*], Luigi Di Sarno[1], Fabio Freddi[2], Mario D'Aniello[3]

[1]*Dept. of Civil Eng. & Industrial Design, University of Liverpool, L69 3GH, Liverpool, U.K.*
[2]*Dept. of Civil, Environmental & Geomatic Engineering, University College London, London WC1E 6BT, U.K.*
[3]*Dept. of Structures for Engineering and Architecture, University of Naples, 80125, Italy*
[*]Corresponding Author. Tel.: +44 7598460022. *Email address:* jingren.wu@liverpool.ac.uk

Abstract

The study described and summarised in this paper was aimed at developing a framework for the definition of force-displacement relationships for single-strut models for masonry infill walls within steel moment-resisting frames. The methodology is based on a genetic algorithm optimisation and can be used for the calibration of force-displacement curves based on databases from either experiments or numerical simulation. A case study is also tested to demonstrate the framework in detail. Due to limited available experimental data on the seismic response of existing steel frames with masonry infills, a set of comprehensive finite element micro-models developed in Abaqus are used to generate a database. The optimal values of the parameters to feed a force-displacement relationship of the single-strut model of the masonry infills are obtained for each micro-model by solving optimisation problems with a genetic algorithm. The optimisation problem involves the minimisation of the discrepancies between the global responses from the database and their corresponding single-strut models through least square minimisation. With the optimal values as the input variables, a generalised quadrilinear model of the masonry strut is obtained through regression analysis and is validated against additional micro-models of infilled steel frames.

Keywords: Moment Resisting Frames, Steel Structures, Masonry Infills, Equivalent strut models, Genetic Algorithm.

1. INTRODUCTION

Masonry infill walls significantly affect the seismic performance of existing moment-resisting frames (MRFs), as demonstrated by several post-earthquake reconnaissance missions and experimental campaigns [1-4]. Existing steel MRFs are often characterised by strong beams - weak columns, and insufficient seismic detailing required to ensure adequate ductility of structures under seismic loading. In some cases, the presence of masonry infills can increase the lateral load resistance and energy dissipation capacities of bare steel frames. However, in other situations, their effects on the structural response can also be detrimental, as they are likely to cause stress concentration at connections. Moreover, they represent a major source of uncertainties in the estimation of structural response. Conventionally, masonry infills are considered as non-structural components in standardised seismic assessment frameworks for steel frames. However, this assumption has been demonstrated to be outdated [5-8]. Although a large number of studies have been carried out on masonry infilled frames, most of them have focused on reinforced concrete (RC) structures while there is still a lack of reliable and practical modelling approaches in current seismic codes to address the issue of masonry infills in the assessment of existing steel frames.

A pioneering contribution to the research of masonry infills on RC structures was provided by Smith [9] and Smith and Carter [10]. The authors performed a series of tests on infill panels and suggested the use of diagonal struts to represent the infill panels in framed structures. Later on, Mainstone [11] experimentally investigated a group of full-scale masonry infill specimens and proposed an equivalent strut model with a simple empirical formula to estimate the effective strut width. Successively, numerous studies have been conducted to numerically investigate the behaviour of infilled steel frames [8, 12-**Error! Reference source not found.**]. In the meantime, many attempts have also been made towards experimental investigations on the behaviour of infilled framed systems (*e.g.*, [15-18]); nevertheless, only a few of them were conducted on steel structures, including mainly monotonic and cyclic quasi-static tests [*e.g.*, 19-25] and more recently a pseudo-dynamic test [26].

Finite element (FE) modelling of masonry infills can be divided into two categories, namely micro- and macro-modelling methods. Micro-models comprise a detailed description of masonry infills, and can accurately capture the responses of infill walls. However, such modelling approach also demands large computational effort and is not suitable for large-scale models. On the other hand, macro-models utilise simplified representations of the geometry of infill wall panels, which is often achieved by modelling the masonry infills as homogeneous isotropic panels or by replacing each infill wall panel with one or more struts in the diagonal directions. Macro-models are

computationally more cost-effective than micro-models, thus being preferrable when only the global response of infilled structures is the main objective of the study.

Equivalent strut models are a widely adopted macro-modelling strategy for masonry infills and can include single- or multiple-struts. Single-strut models utilise one compressive strut in each diagonal of infill wall panels; it is the simplest to build while also capable of capturing the global behaviour of infilled structures with good reliability in many cases. Several single- and multiple-struts models have been proposed in literature, the majority of which were calibrated based on experimental studies on RC structures [*e.g.*, 27-29]. Meanwhile, a limited number of proposals in literature have focused on the modelling of infill walls in steel frames [*e.g.*, 30-32]. Despite being significantly simpler than micro-models, multiple-struts models can still be complex and difficult to implement in the case of large structures characterised, for example, by multiple storeys and spans with varying heights and widths. On the other hand, single-strut models represent a simple and viable alternative to simulate the strength and stiffness contribution provided by masonry infills and to evaluate the global response of infilled structures.

This paper presents a framework that relies on a genetic algorithm to calibrate the properties of masonry single-strut models, which eventually leads to a generalised non-linear force-displacement model for masonry struts incorporated in existing steel MRFs. A case study structure based on a previous experimental test involving a two-storey large-scale existing steel MRF specimen [26] is used to present and demonstrate the framework and the application of the genetic algorithm. Due to the limited numbers of available experimental tests on existing steel frames, the study relies on validated micro-models of infilled steel MRFs. A micro-model of the case study building is initially built as the reference FE model, whose monotonic response is then determined by pushover analysis and validated against experimental results. Successively, based on the calibrated reference micro-model, additional micro-models of existing steel MRFs with varying aspect ratios are built to facilitate the numerical parametric analysis and form a database for performing regression analysis and developing the non-linear force-displacement model for masonry struts.

For the development of the force-displacement model, single-strut models are built, and their properties, which are able best to reproduce the response of the micro-models in the database, are identified through the genetic algorithm (GA). Finally, regression analysis is conducted, and a non-linear force-displacement model for masonry struts is formulated. A detailed description of the methodology is provided in the following section.

2. METHODOLOGY

The framework adopted comprises three main steps, namely *preparation of database*, *calibration of modelling parameters* and *development of regression model*. The analysis framework is schematically demonstrated in Figure 1.

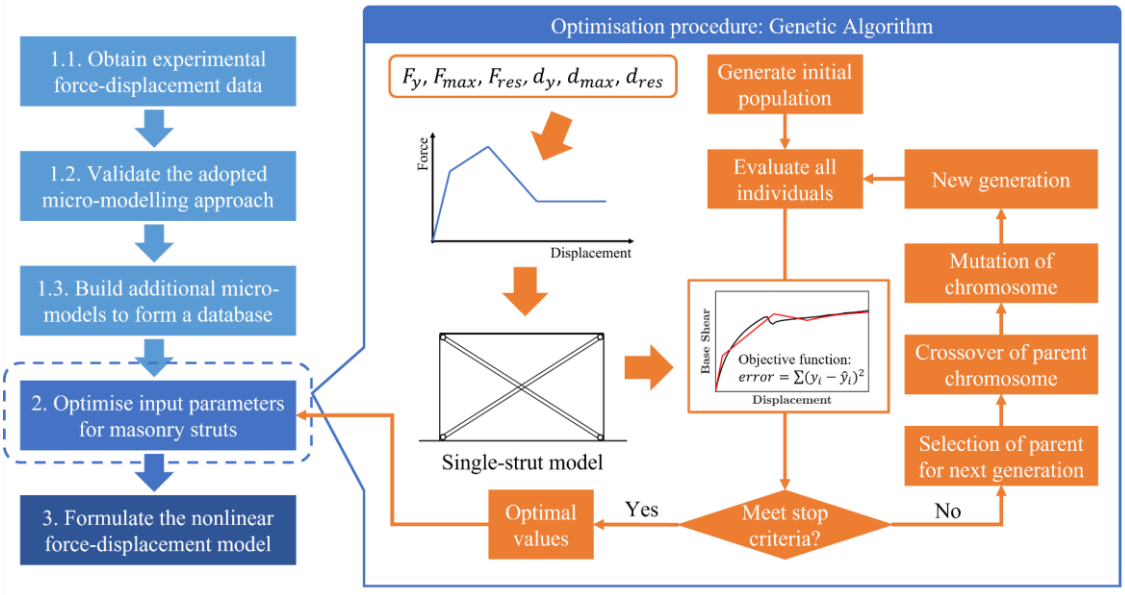

Figure 1. The procedure of developing the force-displacement model for masonry struts.

2.1 Preparation of database

The purpose of this step is to build a database comprising a data set representative of the 'true' force-displacement behaviour of masonry infill walls. The data can be acquired from experimental tests and advanced FE simulations using micro-models of infilled frames. Experimental tests are usually time-consuming and expensive, and hence, integrating the data with those from numerical simulations allows expanding the database for more reliable and comprehensive analyses at the following step.

A database of numerical micro-models is built and utilised to develop data for the local and global responses of masonry infills within steel frames. In particular, given the objective of developing non-linear force-displacement models for the masonry struts, the backbone force-displacement curves of the masonry infills are the responses of principal interest. For this purpose, the micro-models of the infilled frames must be adequately validated in order to gain confidence in the results. Hence, as shown in Figure 1, the generation of such a database includes three sub-steps: (i) to obtain the measured data from a previous experimental test of an existing infilled steel MRF; (ii) to build a calibrated micro-model of the tested steel MRF that is used as the reference model; (iii) to generate additional micro-models based on the reference model by varying the geometric properties of infill walls, and then a database can be assembled. Nevertheless, additional numerical models calibrated against experimental tests using different materials could be successively integrated within the database further to improve the prediction capabilities and generality of the work.

2.2 Calibration of modelling parameters – Genetic algorithm (GA)

In this step, single-strut models are built for each of the micro-models in the database, utilising a generalised force-displacement backbone curve (*e.g.*, a quadrilinear curve in this study) for the masonry struts that is able to accommodate the shape of the global response curves of the micro-models in the database. Then, the optimal backbone curve of each single-strut model is determined by GA [33], which is capable of minimising the discrepancies between the global response curves of the single-strut model and its corresponding micro-model in the database. Thus, at the end of this step, the optimal values of the modelling parameters are determined and are used to serve the regression analysis in the subsequent step.

GA is a machine learning-based method inspired by the natural selection process in biological evolution and is designed for solving both constrained and unconstrained optimisation problems. The major differences between GA and conventional optimisation methods are that GA does not require an initial guess of the variables, and it does not differentiate the objective functions; hence it is particularly useful when the objective is not continuous or differentiable. A detailed description of the genetic algorithm is provided herein.

Definition of the objective function

The first step of applying GA is to build an appropriate objective function to be minimised. In this framework, a general expression of the objective function D is given in Eq.(1), where $\boldsymbol{X}$ is a vector containing all the variables to be optimised, all of which have *positive* values. In GA, $\boldsymbol{X}$ is also known as an *individual* and its entries x_i are known as the *chromosomes*.

$$D = \begin{cases} \sum_{i=1}^{N} \left(F_i - f(\boldsymbol{X})\right)^2 & , g(X) \le 0 \\ \left(\frac{N}{n} \prod_{j=1}^{m} c_i\right) \sum_{i=1}^{N} F_i^2 & , g(X) > 0 \end{cases} \tag{1}$$

When $\boldsymbol{X}$ is a feasible solution, *i.e.*, $g(X) \le 0$, the objective function D is in the form of least squares, where F_i is the benchmark force-displacement behaviour from the database, and $f(\boldsymbol{X})$ is the predicted response. On the other hand, when $\boldsymbol{X}$ represents an infeasible solution, *i.e.*, $g(X) > 0$, the objective function D becomes a penalty function, which deals with two sources of infeasibility. Firstly, the term $c_i = \max\{1, x_i/x_j\}, x \in \boldsymbol{X}$ is used to define the linear constraint between two variables, *e.g.*, the yielding force should be lower than the peak force. Secondly, the term N/n indicates that the first n out of N data points plotting the benchmark curve is simulated by the single-strut model before the analysis failed. This term is used to account for the situation where all linear constraints are satisfied, but an unrealistic solution $\boldsymbol{X}$ leads to non-convergence of the analysis. It is noteworthy

that the penalty function is only activated when an infeasible solution $\boldsymbol{X}$ is being evaluated, which means that the single-strut model failed to provide a complete analysis; thus, the penalty function does not include the response of the single-strut model $f(\boldsymbol{X})$.

Creation of initial population

As illustrated in the right-hand side of Figure 1, GA starts the optimisation process by creating a uniformly distributed initial population of individuals, each individual representing a potential solution $\boldsymbol{X}$, within the bounds of each variable. The creation of random individuals as the initial population is illustrated by Eq.(2).

$$x_{i,j} = l_i + k_{i,j}(u_i - l_i), \qquad k_{i,j} \sim U(0,1) \tag{2}$$

In Eq.(2), $x_{i,j}$ is the i^{th} variable of the j^{th} individual $\boldsymbol{X}_j$ in a population, l_i and u_i are the lower and upper bounds associated with x_i, respectively, and $k_{i,j}$ is a random number generated from the uniform distribution between 0 and 1. The initial population is also referred to as the initial generation, and each time GA creates a new population of individuals by crossover and mutation, the new population is referred to as a new generation, which is similar to the biological evolution.

Evaluation of individuals

For each generation of population, GA firstly calculates the value of the objective function for each of the individuals, normally referred to as the *fitness value*, and then sorts all the fitness values in ascending order. Then GA determines whether the termination criteria are met, which typically includes the maximum allowable number of generations, the minimum relative change in the lowest fitness value over generations, etc. If the criteria are met, the optimal individual is found.

Creation of new population

When the termination criteria are not met, GA continues by creating a new generation, which includes three steps as shown in Figure 1, namely *selection*, *crossover* and *mutation*.

The selection relies on the *fitness score* of each individual in the current generation, which is equal to $1/\sqrt{r}$ based on the rank r of each individual in terms of their fitness values in ascending order. For example, the best individual, which leads to the lowest fitness value, has a fitness score of 1, the second best has a score of $1/\sqrt{2}$, etc. A certain number of individuals in the current generation with the highest fitness scores will directly survive to the next generation, which are known as the *elites*. Subsequently, the roulette wheel method [34] is typically adopted to select the individuals to be parents, which is illustrated in Figure 2a. As can be seen, the individuals with higher fitness scores are more likely to be chosen; nevertheless, those with low fitness scores still have a chance to be parents.

The procedure of crossover is demonstrated in Figure 2b. For each pair of parents, a binary vector is created to decide the chromosomes to be inherited by their child. Meanwhile, some of the parents produce children by mutating their own chromosomes. The mutation normally occurs to one chromosome, and it can be a slight increase or decrease of that chromosome within its bounds. It is noteworthy that the numbers of elites, crossover children and mutation children in the new generation can be customised based on the nature of problems. In the present study, they respectively take up 5%, 75% and 20% of the population containing 200 individuals.

2.3 Development of regression model

In the last step, a regression model is developed for the force-displacement backbone curve of masonry struts. A conventional linear regression is carried out to find the correlation between each of the input parameters for defining the backbone curve and the geometric properties of infill walls (*i.e.*, the aspect ratio). Empirical formulae are provided for the computation of the force-displacement backbone curve and are successively validated against additional micro-models of existing steel MRFs.

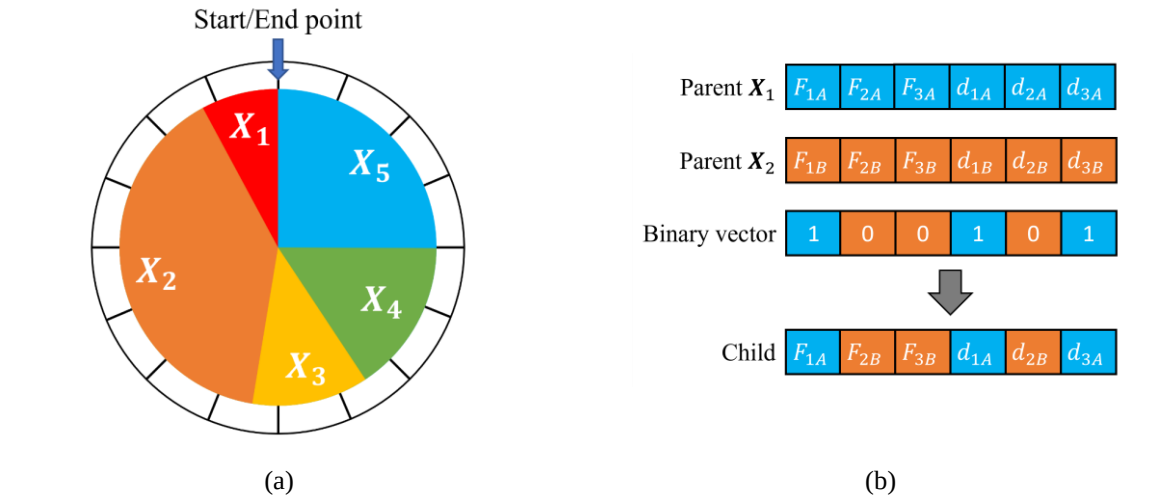

(a) (b)

Figure 2. (a) The roulette wheel selection method; (b) Crossover method based on binary vector.

3. FINITE ELEMENT MODELLING OF INFILLED STEEL FRAMES

3.1 Experimental test and the case study building

The experiment tests carried out by Di Sarno *et al.* [26] were used in this study to calibrate the micro-model of existing steel frames with masonry infills. The case study building is a two-storey steel MRF, which is approximately 5 m in height and spans 6.5 and 3.5 m in the longitudinal and transverse direction, respectively. Sketches of the case study building are provided in Figure 3. The seismic response of the steel MRF was experimentally investigated under a sequence of ground motions through pseudo-dynamic (PsD) tests.

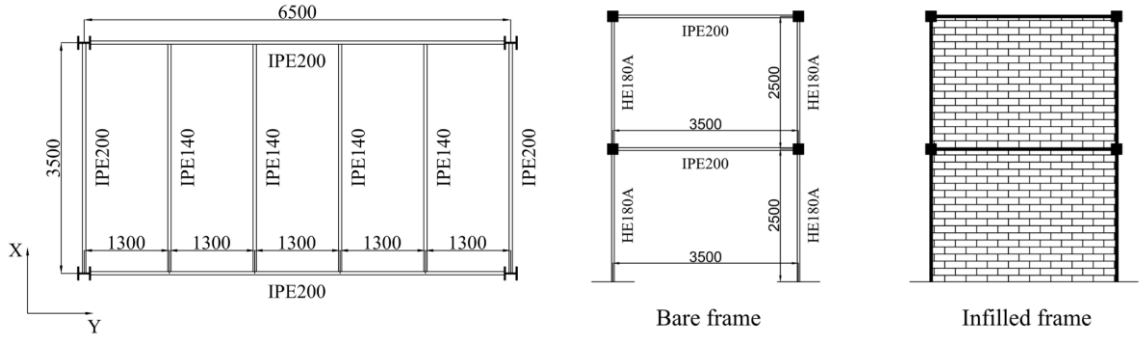

Figure 3. Sketches of the case study steel MRF [26].

The steel MRF was designed to resist mainly gravity loads, thus without adequate code-compliant seismic detailing. The profiles of columns, external beams and internal beams were HE 180A, IPE 200 and IPE 140, respectively. During the construction of the steel MRF, external beams were connected to columns through full penetration welds, where stiffeners were also utilised to increase the rigidity of joints. In the meantime, internal beams were connected to external beams through bolted double angle cleats, as shown in Figures 4a and 4b. Besides, the base of columns was fixed to the strong floor of the lab through thick plates and stiffeners, as shown in Figure 4c, where it can also be seen that two beams with hollow section were placed on top of the base plates to minimise the sliding of column base against the lab's strong floor. In addition, the composite flooring system of the steel MRF consisted of a 150 mm-thick concrete slab poured on 1.25 mm-thick corrugated steel sheets, as shown in Figure 4d, where adequate shear studs were used to ensure full interaction between the slab and beams. The only exception was that in the regions between each beam splice connection and its adjacent column, no shear studs were used in order to avoid the composite actions in the joints. Lastly, the masonry infill walls of the steel MRF consisted of two separate layers of 58 mm-thick brick wall made up of 58×83×190 mm perforated brick unit. The final storey mass of the steel MRF was determined to be 23.5 and 20.0 tons for the first and second

storey, respectively, which accounted for the self-weight, non-structural permanent load and imposed load. The mass corresponding to the additional gravity loads (*i.e.*, the non-structural permanent load and imposed load) was simulated by placing concrete blocks with equivalent self-weight on the slab of each storey, as shown in Figure 4e. The actuators and their connections to the steel frame are also shown in Figure 4f.

The mechanical properties of the structural steel were acquired by means of coupon tests, while compression and shear tests were carried out to obtain the properties of the masonry infills. The mean measured yield strength of steel is about 423.78 MPa. The mean compressive ultimate strength of masonry infills in the direction perpendicular to the bed joints is equal to 2.81 MPa, and the diagonal tensile strength is 0.65 MPa.

(a) (b) (c)

(d) (e) (f)

Figure 4. The case study building tested in the lab [26].

3.2 Micro-modelling of the case study infilled frame

A 3D finite element (FE) model of the case study structure was built in Abaqus [35]. The modelling procedure followed the simplified micro-modelling approach [36, 37]. To reduce the demand for computational cost, the FE model included only a sub-structure of the steel frame, *i.e.*, half of the first storey, instead of the entire structure.

The details of the FE model are shown in Figure 5. All steel components (i.e., beams, columns, plates, and stiffeners) were modelled as solid elements (C3D8R). The Young's modulus and Poisson's coefficient of steel were assumed to be 210 GPa and 0.3, respectively, and a perfectly plastic post-yielding behaviour was adopted. Besides, the external beams were connected to columns using tie constraints to simulate the full penetration welds, while the internal beams were omitted from the FE model as they did not significantly affect the response of the steel MRF when a rigid slab was present in the model. Similarly, steel plates and stiffeners were connected to beams and columns using tie constraints.

Aside from the steel members, the concrete slabs in the FE model, including the concrete base supporting the infill walls on the ground, were modelled using solid elements (C3D8R). Both the composite slab and the reinforced concrete base were simplified as homogeneous concrete blocks with an equivalent Young's modulus to simulate the rigidity of the internal beams and slabs as composite sections. Plastic behaviour was not defined for concrete in the present study since no cracking was observed in the concrete components of the case study building during the PsD test. The slab was connected to the top flange of external beams through tie constraints in the region where shear studs were present, while in the absence of shear studs, contact was defined between the slab and beam, which comprised tangential behaviour with a friction coefficient of 0.7 and 'Hard' normal behaviour.

The masonry infills consisted of expanded brick units, each representing an original brick unit plus half of the thickness of mortar on each side and the brick-mortar interface. The expanded brick unit was modelled as a continuum element (C3D8R) and was placed in the same way as the real infill walls in the steel MRF. The Young's modulus of the expanded brick unit was assumed to be equal to the adjusted Young's modulus of the masonry assemblage in the steel MRF (*i.e.*, the entire infill wall), which was determined based on the formula proposed by Abdulla *et al.* [36], as given in Eq.(3). H_m is the height of masonry assemblage, E_u and E_{mo} are the Young's modulus of the brick unit and mortar, H_u and H_{mo} are the height of brick unit and thickness of mortar, and n is the number of courses in a masonry assemblage. The elastic properties of brick, mortar and masonry assemblage are summarised in Table 1. The Young's modulus of brick and mortar were assumed to be 21500 and 2550 MPa, respectively, due to lack of experimental data. This assumption yielded a Young's modulus of 7688 MPa for the masonry triplet involved in the compressive test, which was consistent with the experimental measurement. Moreover, the Concrete Damage Plasticity model was used to describe the inelastic behaviour of the expanded brick unit. The ultimate strength in tension and compression was set to be 0.65 and 2.81 MPa, respectively, according to the results of material tests. It should also be noted that fracture energy of 0.05 Nmm/mm^2 was adopted to define the failure of masonry in tension, according to da Porto *et al.* [38].

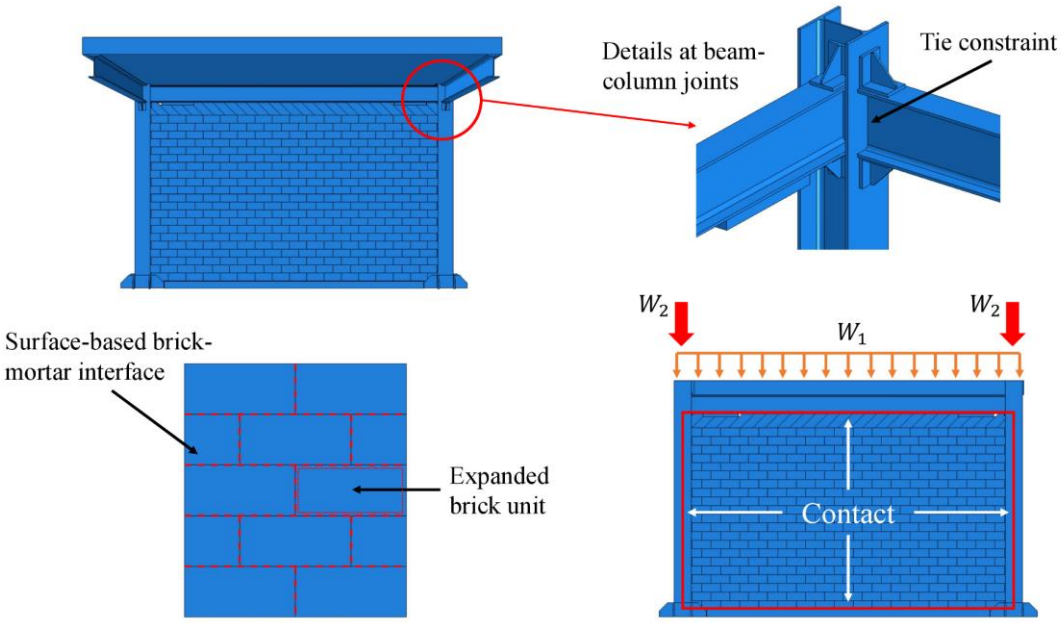

Figure 5. Description of the meso-model of the infilled steel MRF in Abaqus.

$$E_{adj} = \frac{H_m E_u E_{mo}}{nH_u E_{mo} + (n-1)H_{mo}E_u} \tag{3}$$

Table 1. Material properties to build the model of the brick unit.

	n	Height (mm)	Young's modulus (MPa)
Brick	1	83	21500*
Mortar	-	10	2550*
Masonry triplet (Material test)	5	269	7688
Infill wall	45 ~ 47	2129 ~ 2222	6148 ~ 6141

On the other hand, the cohesive behaviour of the brick-mortar interface was modelled by employing the surface-to-surface contact approach. The cohesive behaviour was described through the traction-separation law shown in Figure 6. The elastic response was defined by Eq.(4), where $\boldsymbol{t}$ is the traction stress vector, $\boldsymbol{\delta}$ is the separation vector, and $\boldsymbol{K}$ is the stiffness matrix. The components of the stiffness matrix $\boldsymbol{K}$ were calculated using the

expressions in Eq.(5) and Eq.(6), where G denotes the shear modulus. Besides, the damage initiation of the cohesive behaviour was controlled by the quadratic stress criterion given in Eq.(5), where the use of the Macaulay bracket excluded the effects of compressive stress on the damage of the interface in the normal direction. In the present study, the tensile strength (t_n^{max}) and shear strength (t_s^{max} and t_t^{max}) were calibrated based on the diagonal compressive test of masonry triplets reported in [26]. Additionally, damage evolution was defined in terms of fracture energy, adopting the Benzeggagh-Kenane law [39] with a power of 2.0 and linear softening. Due to the lack of relevant experimental data, the fracture energies for normal and shear traction were defined according to Lourenço [40]. The parameters describing the interfaces' elastic and inelastic cohesive behaviour are summarised in Tables 2 and 3, respectively. The cohesive behaviour was employed in conjunction with 'Hard' normal behaviour and tangential behaviour (μ = 0.75) for the definition of the contacts between brick units (*i.e.,* the head joints and bed joints of bricks).

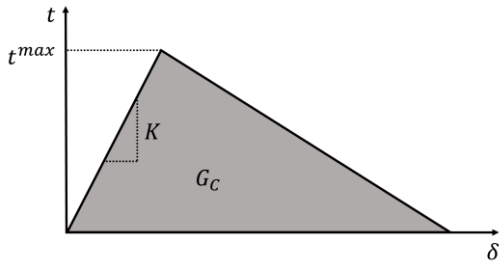

Figure 6. Traction-separation behaviour of the brick-mortar cohesive joints.

$$\boldsymbol{t} = \begin{bmatrix} t_n \\ t_s \\ t_t \end{bmatrix} = \begin{bmatrix} K_{nn} & 0 & 0 \\ 0 & K_{ss} & 0 \\ 0 & 0 & K_{tt} \end{bmatrix} \begin{bmatrix} \delta_n \\ \delta_s \\ \delta_t \end{bmatrix} = \boldsymbol{K\delta} \tag{4}$$

$$K_{nn} = \frac{E_u E_{mo}}{H_{mo}(E_u - E_{mo})} \tag{5}$$

$$K_{ss} \text{ and } K_{tt} = \frac{G_u G_{mo}}{H_{mo}(G_u - G_{mo})} \tag{6}$$

$$\left(\frac{\langle t_n \rangle}{t_n^{max}}\right)^2 + \left(\frac{t_s}{t_s^{max}}\right)^2 + \left(\frac{t_t}{t_t^{max}}\right)^2 = 1 \tag{7}$$

Table 2. Stiffness adopted in the traction-separation model.

K_{nn} (N/mm^3)	K_{tt} (N/mm^3)	K_{ss} (N/mm^3)
290	116	116

Table 3. Parameters to define the damage initiation and evolution in the traction-separation model.

t_n^{max} (MPa)	t_t^{max} (MPa)	t_s^{max} (MPa)	G_n^C (Nmm/mm2)	G_t^C (Nmm/mm2)	G_s^C (Nmm/mm2)
0.8	2.4	2.4	0.01	0.03	0.03

Finally, the contacts between the infill walls and the confining frame were modelled with 'Hard' normal behaviour and tangential friction with μ = 0.7 between masonry and concrete (at the base), and μ = 0.3 between masonry and steel (with columns and the upper beam). The determination of the friction coefficients was based on typical values between relevant surface types, which were consistent with the range of values reported in Lourenço [40] and were validated in the following section. Meanwhile, fixed boundary conditions were imposed to the bottom of columns and the concrete base, while symmetric boundary conditions were also applied to the ends of slab and the transverse beams. Lastly, as the present study focuses on the in-plane behaviour of masonry infills, lateral

restraints were also employed to the infill wall panels. This assumption is consistent with the experimental evidence where out-of-plane response was not observed within the range of drifts of interest in this study.

3.3 Validation of the reference FE model

The numerical simulations were performed with 2 steps: the Gravity and the Pushover analysis. The gravity loads shown in Figure 5 were included to indirectly account for the presence of the second storey of the structure experimentally tested and which was not included in the FE model. The vertical loading is known to affect the behaviour of infill walls by modifying the deformed shape of beams and columns and correspondingly changing the contact length between the infill walls and surrounding frames [41], thus it is essential to properly simulate the realistic vertical loading condition.

Successively, a Pushover analysis was performed on the FE model, from which the storey shear-drift curve was obtained and then compared with the experimentally measured response. The Pushover analysis was conducted by applying incremental horizontal displacement to the control point, i.e., the geometric centre of the slab top surface, for up to 40 mm, which corresponded to approximately 1.75% of inter-storey drift ratio. The control point enforced the top surface of the slab to undergo the same horizontal displacement through *coupling* constraint. *Quasi-static* analysis in the *implicit dynamic* analysis category was selected for the Pushover analysis. It is worth noting that the Pushover analysis was conducted in both the positive and negative directions, allowing better comparison with the cyclic response of the test specimen.

The comparison between the numerical and experimental curves is presented in Figure 7, showing a good agreement between the numerical and experimental results in terms of the peak force. It is worth mentioning that the post-peak strength deterioration was not fully captured, as the FE model was not able to simulate accurately some of the local responses observed during the test, *i.e.*, the crushing of the masonry infill bricks close to the beam-column connections. It can also be seen from Figure 8 that the estimated damage on the masonry wall by the FE model is also similar to the actual damage observed in the laboratory.

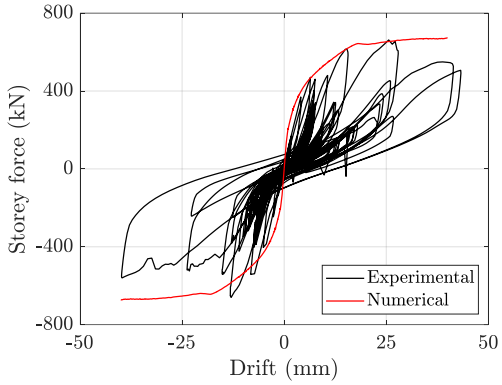

Figure 7. Comparison of the storey force-drift behaviour of the case study building obtained from numerical simulation and experimental measurement.

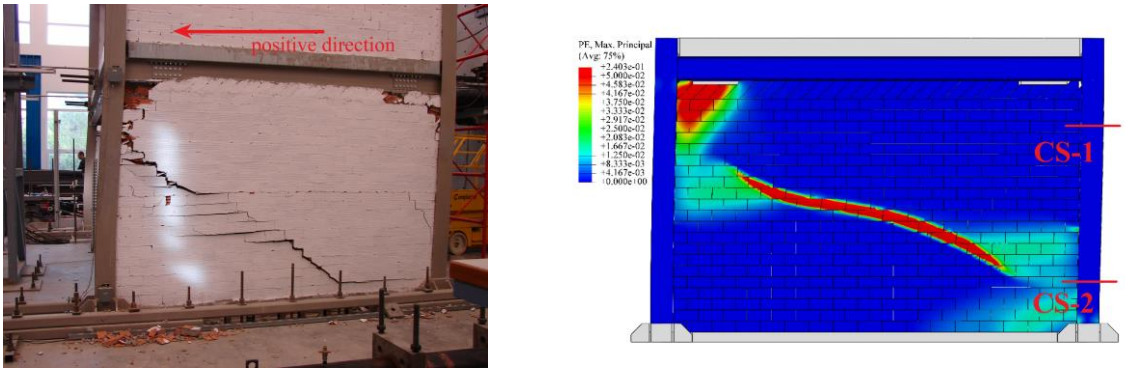

(a) (b)

Figure 8. Comparison of the damage observed on the masonry wall (maximum absolute principle plastic strain).

Additionally, in order to validate the FE model, comparisons were also made in terms of bending moments measured at two cross-sections of the right column, as shown in Figure 8b. These cross-sections are 400 mm below the bottom of the upper steel beam (*i.e.*, Cross-section 1) and below the top of the base stiffeners (*i.e.*, Cross-section 2). The comparison of the bending moments is presented in Figure 9, which shows the bending moment induced by the lateral loading only, *i.e.*, the contribution from the gravity loading was filtered. It can be seen that the numerically predicted bending moment satisfactory matches the corresponding experimentally measurements. It is also of interest to notice that the column-infill wall interaction over the contact length had a larger impact on the top part of the column than on the bottom part in terms of its flexural behaviour. This is because the moment at Cross-section 1 firstly increased in the positive direction before the damage occurred in the top-right corner, which caused the moment at Cross-section 1 to start increasing in the negative direction. This suggested that the horizontal load applied to the column by the infill's strut action over the contact length was larger at the top part of the column than at the bottom of the column. Nevertheless, it can also be seen from Figure 9 that the moment demands were more critical at the bottom of the column.

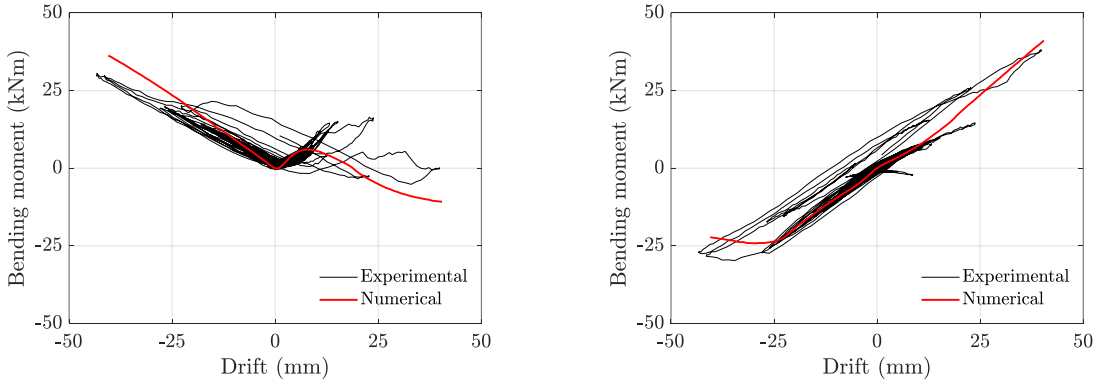

(a) (b)

Figure 9. Comparison of the bending moment in column: (a) Cross-section 1; (b) Cross-section 2 (See Figure 8).

3.4 Generation of additional micro-models to build the database

A numerical parametric analysis was conducted using the previously validated FE model to create the case study masonry infilled steel frames database. A total of nine models were created covering different spans (L) and heights (H) of the steel frame, and hence different widths (L_{Infill}), heights (H_{Infill}) and aspect ratios ($(L/H)_{Infill}$) of the masonry infill walls, as summarised in Table 4. All the models were built adopting the same material properties as the FE model of the test specimen. Besides, all the models built for the parametric analysis adopted the same profiles for the steel members as those for the test frame, two layers of brick walls made of the same brick units, as well as a 150 mm-thick concrete slab. It is worth mentioning that an elastic concrete slab was also assumed in the numerical models for the parametric analysis, in order to reduce the computational effort. The validity of this assumption was checked by monitoring the values of the concrete stress during each numerical simulation. All the models were subjected to Gravity and Pushover analysis, with the same target displacement of the control point of 50 mm, to acquire their monotonic force-displacement behaviour.

Figure 10 shows the stress distribution in the masonry infill wall panel in each of the FE models at their peak strength. For all models, the damage was first observed in the infill walls' central area, as indicated by the loss of stress within the compressive zone of the masonry infills. This is likely attributed to the relatively weak column joints compared to the masonry infill. Besides, it is also clearly shown that the aspect ratio greatly impacts the behaviour of masonry infill walls in steel frames, and the compressive diagonal struts created in the FE models can be divided into three categories. Firstly, in Model-1, -4 and -7, whose aspect ratios are the largest among all the models, a small off-diagonal strut can be observed in addition to the main diagonal strut. It can also be seen that the small strut tended to be less significant when the aspect ratio decreased. Secondly, in Model-2, -5, -8 and -9 with intermediate aspect ratios, a single strut with damage in the centre of the wall panel was noticed, and the aforementioned small strut disappeared in these four cases. Lastly, in Model-3 and -6, whose aspect ratios are the smallest, a clear two-strut mechanism was noticed compared to other models, which then further propagated into a more complex damage pattern.

Table 4. Geometric properties of the infilled steel frame models used for the database.

Model	E_{adj} (MPa)	L (mm)	H (mm)	L_{Infill} (mm)	H_{Infill} (mm)	$(L/H)_{Infill}$ (-)
Model-1	6135	3506	2575	3500	2325	1.505
Model-2	6135	2906	2575	2900	2325	1.247
Model-3	6135	2306	2575	2300	2325	0.989
Model-4	6150	3506	2389	3500	2139	1.636
Model-5	6150	2906	2389	2900	2139	1.356
Model-6	6150	2306	2389	2300	2139	1.075
Model-7	6165	3506	2203	3500	1953	1.792
Model-8	6165	2906	2203	2900	1953	1.485
Model-9	6165	2306	2203	2300	1953	1.178

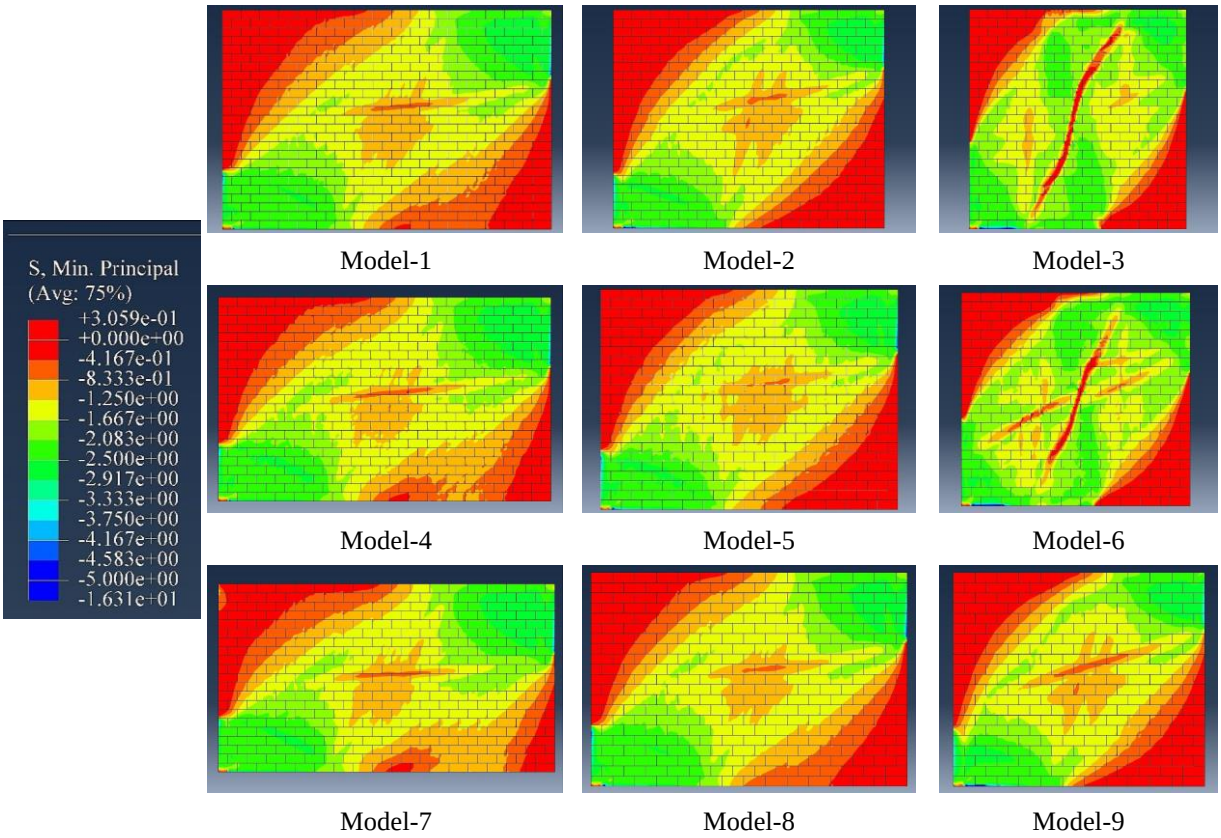

Figure 10. Stress contour of masonry infill walls (steel and concrete members are omitted for clarity).

The force-displacement curves of the nine models are summarised in Figure 11a, while Figure 11b shows the net contribution due to masonry infills, which were determined as the total base shear subtracted by the contribution from the bare frame. It can be seen from Figure 10b that almost all models are characterised by a clear drop of strength in their lateral force-displacement response. In Model-7, however, the reduction in strength is quite limited, which is likely due to the fact that this model had the most significant off-diagonal strut that compensated the majority of stress loss due to the damage in the main strut. Additionally, Model-3 and -6 exhibited a slight drop of strength before their strength rose again by around 10% to reach the peak force. These differences clearly show the significant influence of the aspect ratio on the response of infill walls and the different mechanisms developed to resist horizontal loads.

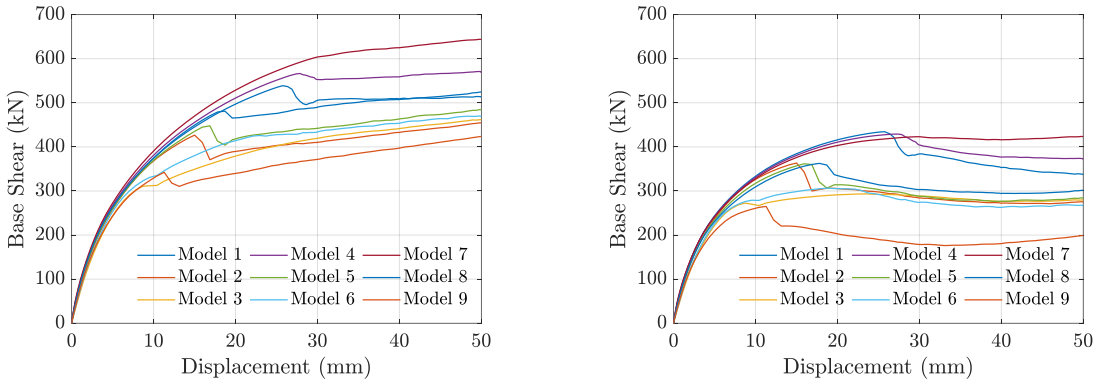

Figure 11. Global response of the micro-models: (a) infilled frames (the force was doubled as only half the frame was built in the micro-model); (b) net contribution of all infills.

In addition to the global response, Figure 12 shows the shear force and bending moment diagrams of both the windward ("W") and leeward ("L") columns of Model-2, -6 and -7, individually at the peak force of the masonry infill walls. It is necessary to highlight that the masonry infills are not included in Figure 12 for clarity, despite their presence in the micro-models. These three models were selected for illustration purposes as they are representative of cases with the largest, intermediate and smallest aspect ratios as discussed above. As shown in Figure 12, the steel frames were pushed to the left-hand side, thus the column on the right-hand side was the windward column, while the one on the left was the leeward column. Besides, all the diagrams in Figure 12 were plotted in terms of shear forces and bending moments, normalised respectively with respect to the shear capacity and plastic moment capacity determined according to the Eurocode 3 [42]. It can be seen that in all cases, the maximum shear force demands occurred at the top of windward columns and the bottom of leeward columns due to the strut action of the masonry walls. It is also noticed that the shear force demands at the bottom of leeward columns were approximately 25% lower than the shear force demands at the top of windward columns, which was attributed to the higher friction coefficient between the wall and the concrete base; thus, a larger portion of the horizontal force was transferred through the friction. On the other hand, as shown in the bending moment diagrams, when the masonry infills reached their load capacities, the maximum bending moment demands were all found at the bottom of leeward columns, which was in general significantly higher than anywhere else in the two columns. Consistent results have been observed in all the other cases that are not reported here for the sake of brevity.

4. DEVELOPMENT OF THE FORCE-DISPLACEMENT MODEL

4.1 Calibration of the optimal values of input parameters

In order to build simplified models of the infilled steel frames considered in this numerical parametric study, the single-strut model was adopted to simulate the infill walls due to its simplicity. The simplified models of the infilled frame were created in the finite element software *OpenSees* [43].

A schematic view of the modelling of infilled steel frames in OpenSees is provided in Figure 13. Columns were modelled according to a distributed plasticity approach and considering the *Steel01* material in OpenSees with a yield stress of 423.78 MPa and post yielding hardening of 0.001 to simulate the elastic-perfectly plastic behaviour (consistent with the micro-models). Conversely, beams were modelled using a lumped plasticity approach with elastic elements and non-linear rotational springs at beams' ends. Plastic hinges were modelled using moment-rotation relationships defined according to Lignos and Krawinkler [44] and Zareian and Medina [45]. The behaviour of the rotational spring is presented schematically in Figure 14a, with detailed data reported in Table 5. In addition, connections were considered fully rigid in the simplified models, and fixed restraints were applied to all column bases.

The masonry struts were modelled using truss elements whose properties in the horizontal direction were directly described by a quadrilinear force-displacement relationship, which was able to represent all the force-displacement curves shown in Figure 11b. The quadrilinear curve is shown in Figure 14b, with the subscript 'h' denoting horizontal behaviour, and describes the response of masonry infills at four phases: *1)* the linear elastic

behaviour of the infills; *2)* the reduced stiffness of the infill due to cracking; *3)* the strength softening of the infills; *4)* the residual strength of the infill.

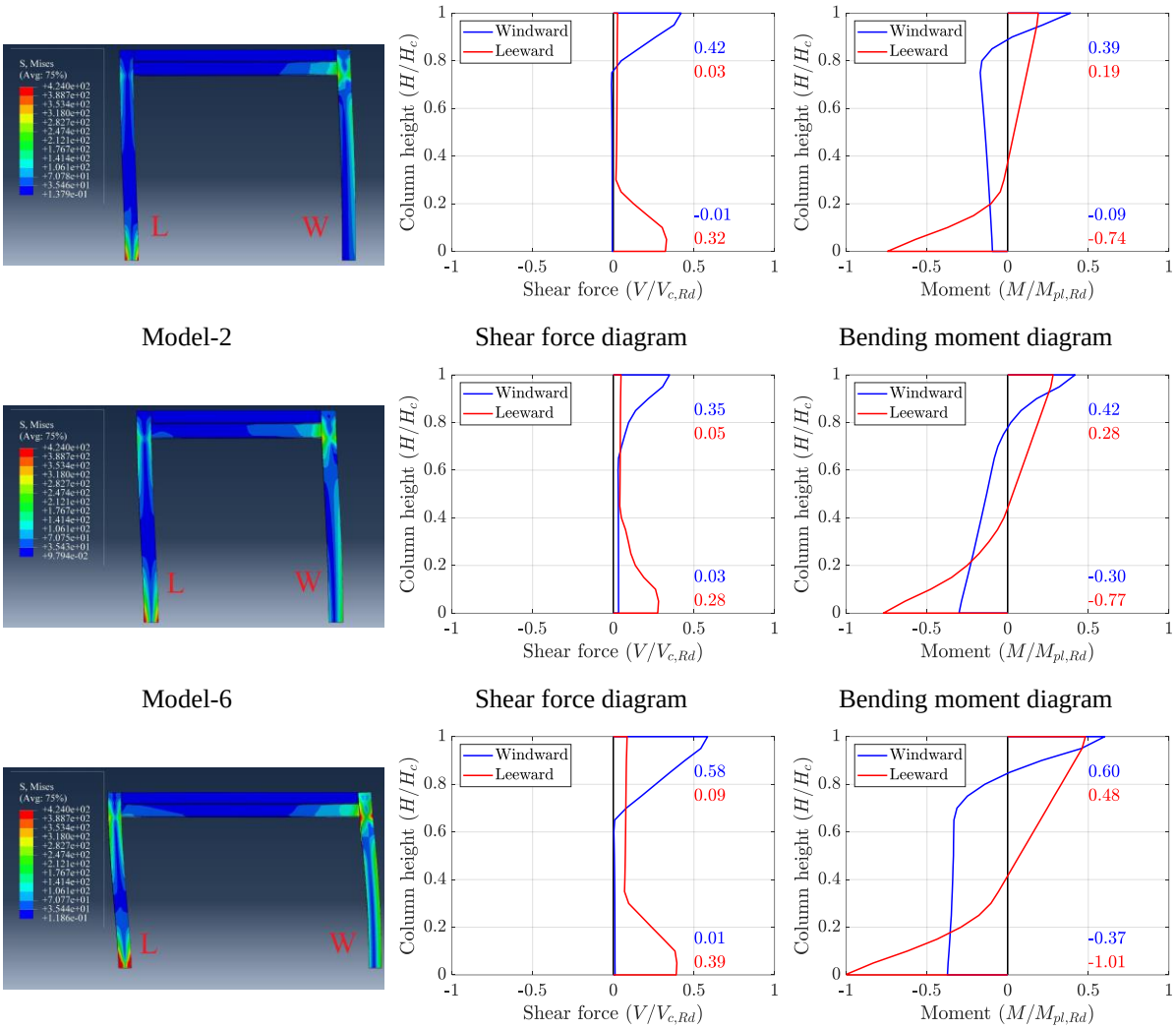

Model-2 Shear force diagram Bending moment diagram

Model-6 Shear force diagram Bending moment diagram

Model-7 Shear force diagram Bending moment diagram

Figure 12. Shear force and bending moment diagrams of the columns (masonry walls and concrete base omitted for clarity).

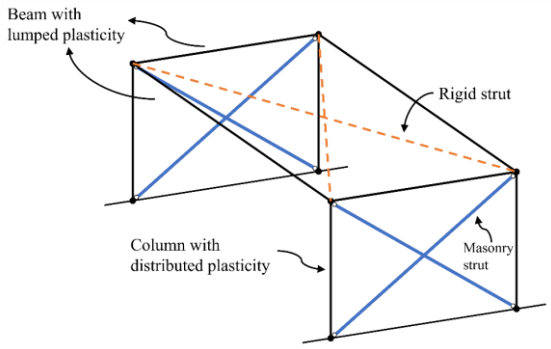

Figure 13. Schematic view of the frame with masonry infills modelled as single-struts in OpenSees.

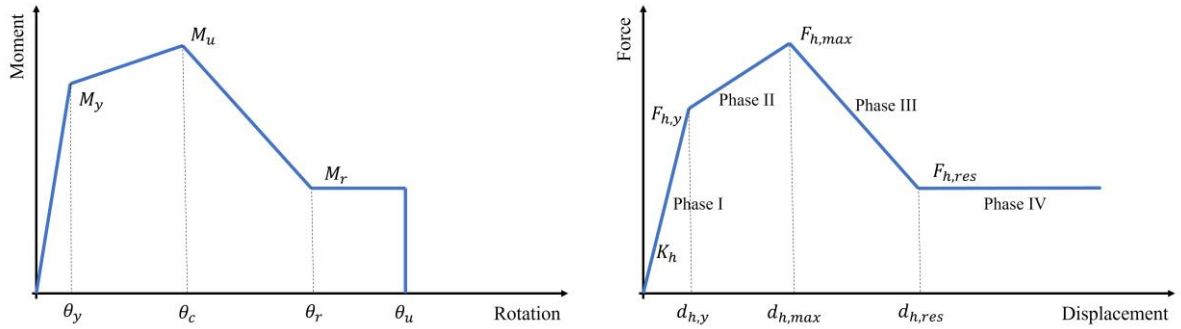

(a) (b)

Figure 14. Backbone curves implemented in the OpenSees models: (a) beam plastic hinges (see Table 5); (b) masonry struts.

Table 5. Parameters to define the backbone curve for the beam plastic hinges.

M_y (kNm)	M_u (kNm)	M_r (kNm)	θ_y (rad)	θ_c (rad)	θ_r (rad)	θ_u (rad)
93.82	101.16	37.68	0.002	0.082	0.239	0.332

The definition of the quadrilinear curve requires the determination of six parameters, including the elastic stiffness (K_h), yielding force ($F_{h,y}$), peak force ($F_{h,max}$) and residual force ($F_{h,res}$), and their corresponding displacements ($d_{h,max}$ and $d_{h,res}$), as shown in Figure 14b. Among the six parameters, the elastic stiffness K_h and the peak force $F_{h,max}$ can be directly obtained from the response of infills in Figure 11b due to superposition, which are denoted as $K_{h,0}$ and $F_{h,max,0}$, respectively. Therefore, to perform GA optimisation, the individual was expressed as $X = [F_{h,y} \quad F_{h,res} \quad d_{h,max} \quad d_{h,res}]^T$.

The lower and upper bounds of the four parameters were summarised in Table 6. It is worth mentioning that since there were a total of four panels in the whole infilled frame, *i.e.*, two brick panels in one wall, the upper bound of the yield and residual force of the infilled frame was set to be $F_{h,max,0}/4$. Meanwhile, the displacement variables were given an upper bound of 50 mm. The determination of this value was a trade-off between the computational demand and the fitness of $d_{h,res}$, but should not underestimate the displacement at peak force $d_{h,max}$. In addition to the bounds of the variables, the definition of the ratios a_i in the penalty function is also reported in Table 6, which considered five constraints. Among them, c_1 and c_3 constrained the yield displacement to be smaller than the peak displacement, and the peak displacement to be smaller than the residual displacement, and c_2 constrained the secant stiffness at peak force to be smaller than the initial stiffness. Successively, GA performed the optimisation task based on the objective function *D* in Eq.(1), where the least squares were calculated based on the global response shown in Figure 11a. The solutions are presented in Figure 15, and the optimal values are reported in Table 7.

Table 6. Upper and lower bounds of the variables to be optimised and associated constraints.

Parameter	Upper bound	Lower bound	$c_i = \max\{1, x_i/x_j\}$
$F_{h,y}$	$F_{h,max,0}/4$	0	$c_1 = \{1, \frac{F_{h,y}/K_h}{d_{h,max}}\}$
$F_{h,res}$	$F_{h,max,0}/4$	0	N/A
$d_{h,max}$	50 mm	0	$c_2 = \max\{1, \frac{F_{h,max,0}/d_{h,max}}{K_{h,0}}\}$
$d_{h,res}$	50 mm	0	$c_3 = \{1, \frac{d_{h,max}}{d_{h,res}}\}$

Table 7. Optimal values of the parameters to define the backbone curve of masonry struts.

Model	K_h (kN/mm)	$F_{h,y}$ (kN)	$F_{h,max}$ (kN)	$F_{h,res}$ (kN)	$d_{h,y}$ (mm)	$d_{h,max}$ (mm)	$d_{h,res}$ (mm)
Model-1	28.74	60.42	108.52	85.04	2.10	25.02	36.21
Model-2	23.84	49.67	90.12	65.47	2.08	14.54	27.91
Model-3	18.41	59.15	73.46	67.67	3.21	22.34	36.54
Model-4	29.70	61.13	107.82	92.42	2.06	26.59	35.32
Model-5	24.87	48.65	90.09	68.56	1.96	15.25	27.02
Model-6	19.36	56.43	76.94	64.59	2.91	18.45	33.97
Model-7	30.70	63.99	106.37	102.66	2.08	29.78	36.99
Model-8	26.04	49.50	90.57	72.13	1.90	17.37	28.34
Model-9	20.18	43.34	65.54	44.05	2.15	11.27	25.56

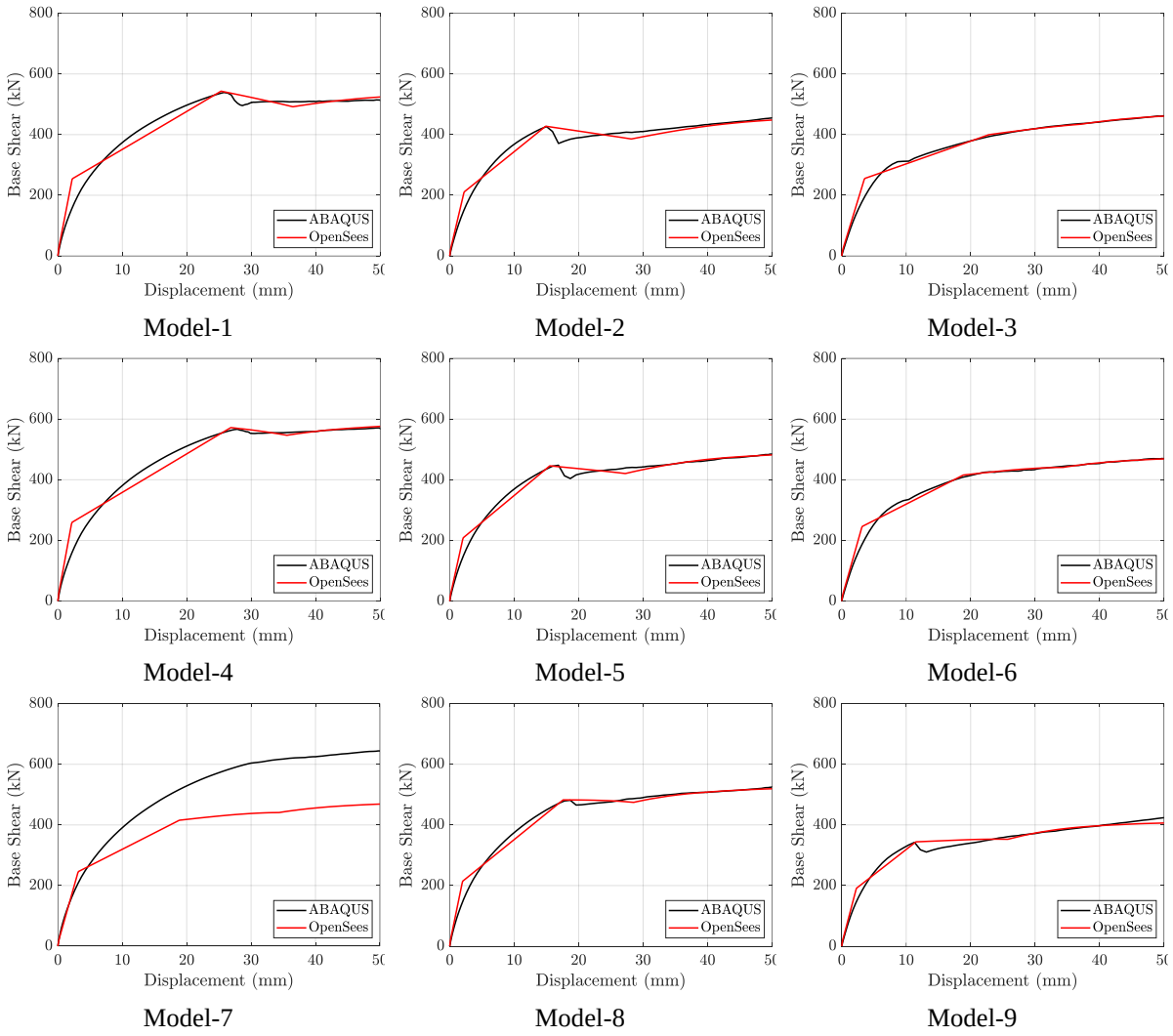

Figure 15. Comparisons between the global resposne of the micro-models in Abaqus and their corresponding simplified models in OpenSees.

In addition to the global response, the single-strut OpenSees model's ability to simulate the local responses was also investigated. Figure 16 shows the shear force diagrams at the peak force of infill walls for the windward and leeward columns. In the plots, 'C' denotes force in the column, while 'M' denotes the horizontal component of the force in the masonry strut. These plots clearly show that the single-strut model cannot adequately simulate the shear force demand on columns, significantly underestimating it by approximately 80%, either in the windward or leeward columns. This is related to the simplifications made in the arrangement of the single-struts that were directly connected to the columns' end nodes, not accounting for the masonry infill-column contact length. In order to evaluate the force in masonry struts, its horizontal component acting on the end nodes of columns is also presented in Figure 16. It can be seen that the sum of the shear force in columns and the horizontal component of the force in masonry struts are much closer to the shear force demands estimated by the micro-models, which were approximately 20% underestimated for windward columns but almost identical for leeward columns.

In a similar manner, Figure 17 shows the comparisons of bending moment diagrams. The results show that the moment demands in windward columns were generally predicted by the single-strut model with less than 15% discrepancies. However, for the leeward columns, which were more critical in terms of moment demand, maximum moments were underestimated by the single-strut model by 15 to 50%. Also in this case, this is due to the arrangement of the single-struts within the models. To sum up, as expected, the single-strut model was able to reproduce the global response of the infilled steel MRFs accurately but failed to predict the shear force and moment demands in columns. However, despite some well-known limitations, single-strut models are widely adopted by engineers and implemented in the codes of practice thanks to their great simplicity.

4.2 Regression analysis

The above-discussed models were calibrated to simulate the lateral response of the investigated cases, but no formulations have been yet provided to generalise the single-strut models. The following part of this paper tries to address this issue by investigating a strategy for the definition of horizontal force-displacement models for the masonry strut by using regression analysis. As previously discussed, the aspect ratio was found to significantly affect the formation of compressive struts within the infill wall panel, and hence this parameter was taken as the main predictor in the present regression analysis. The formulation of the horizontal force-displacement relation model for the masonry strut is illustrated by Eq.(8) to Eq.(15), which involves six coefficients (α, β, a_1, a_2, b_1 and b_2) to be determined based on regression analysis. A detailed description of the model is provided herein. It is noteworthy that the forces and the displacements discussed in this part are related to the horizontal direction.

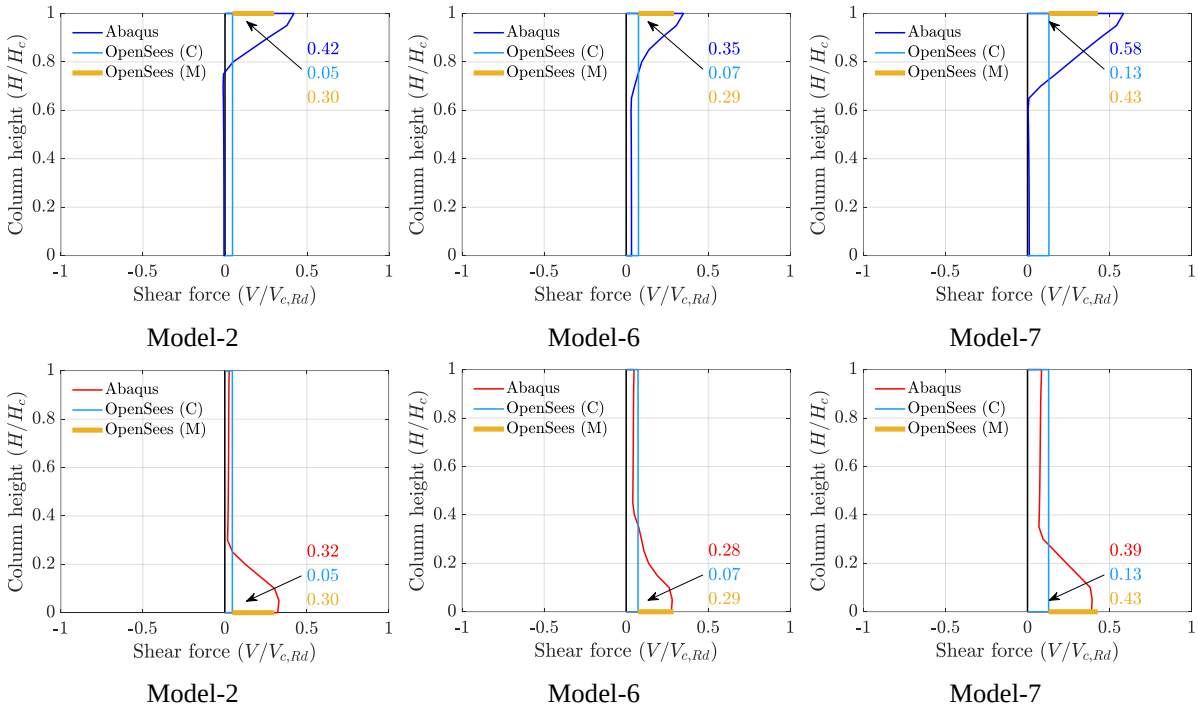

Figure 16. Comparisons of shear force diagram of windward columns (top) and leeward columns (bottom) obtained from the Abaqus and OpenSees models.

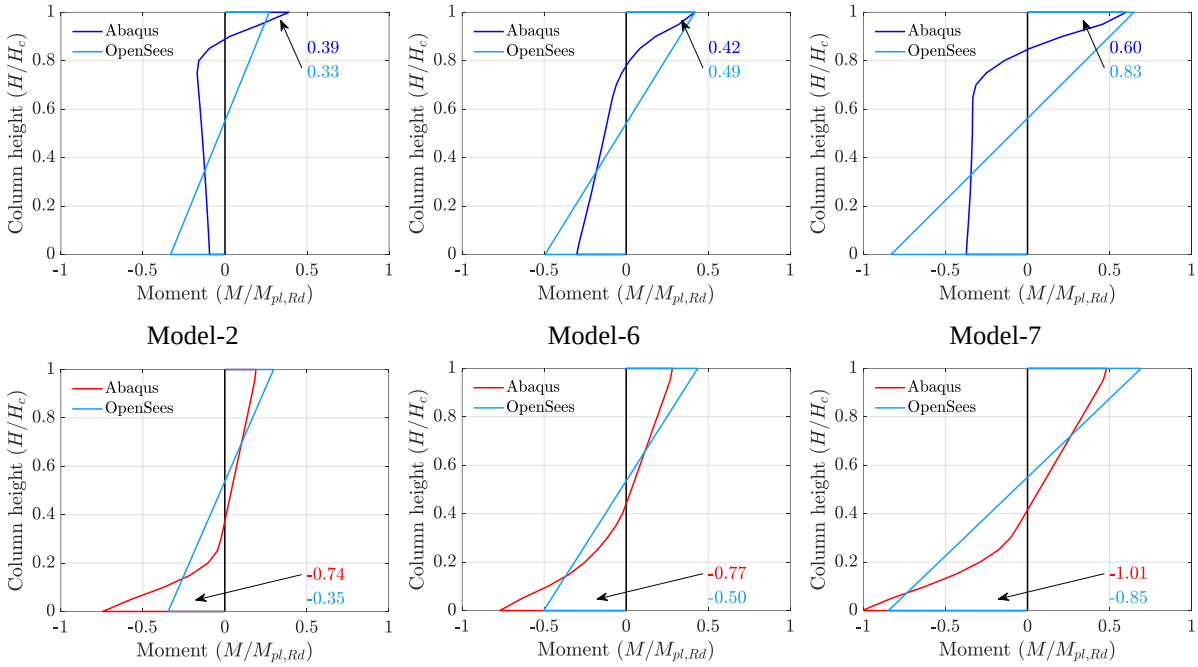

Figure 17. Comparisons of bending moment diagram of windward columns (top) and leeward columns (bottom) obtained from the Abaqus model and the OpenSees model.

I. Elastic stiffness and strut width

The elastic stiffness of the masonry strut can be defined by Eq.(8) where E_m is the Young's modulus of the masonry strut, t_m is the thickness of the infill wall and L_m/H_m is the aspect ratio of the wall panel. The use of this formula was based on the assumption that for small drifts, the infill wall is in full interaction with the confining frame with no cracking, and hence the response of the masonry wall depends on its shear behaviour. A single coefficient α was included to account for both the linear relation between the Young's modules E_m and the Shear modules G_m and the loading condition. In this way, the strut width b_m in the present study could also be obtained by relating it to the elastic stiffness, as given in Eq.(9), where d_m is the length of the masonry strut, and θ is the angle between the strut and the beam.

$$K_h = \alpha E_m t_m \frac{L_m}{H_m} \tag{8}$$

$$b_m = \alpha \left(\frac{L_m}{H_m}\right) \frac{d_m}{cos^2\,\theta} \tag{9}$$

II. Peak force

The load-carrying capacity of the masonry strut can be defined by Eq.(10) where f_m is the shear strength of the masonry infill measured by diagonal compressive tests, and $t_m L_m$ is the area of the horizontal cross-section of the masonry wall. A coefficient β was included to account for the variation of aspect ratios of infill walls. This formula was chosen because, in a preliminary investigation of the correlation between the peak force and all potential independent variables, it was found that the peak force showed a strong linear correlation with the width of the wall L_m as demonstrated in Figure 18. Based on this observation, it is anticipated that the coefficient β may be approximated as a constant.

$$F_{h,max} = \beta f_m t_m L_m \tag{10}$$

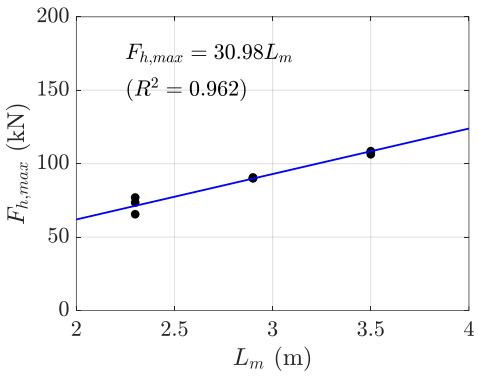

Figure 18. Load-carrying capacity of masonry strut ($F_{h,max}$) vs. the width of walls (L_m).

III. Yielding and residual force

The yielding and residual forces of masonry strut can be obtained by relating them to the peak force through the coefficient a_1 and a_2, respectively, as given in Eq.(11) and Eq.(12).

$$F_{h,y} = a_1 F_{h,max} \tag{11}$$

$$F_{h,res} = a_2 F_{h,max} \tag{12}$$

IV. Displacements

The three displacement parameters of the quadrilinear force-displacement model can be determined by Eq.(13) to (15), where b_1 and b_2 are the coefficients that relate peak and residual displacements to the yielding displacement.

$$d_{h,y} = \frac{F_{h,y}}{K_h} \tag{13}$$

$$d_{h,max} = b_1 d_{h,y} \tag{14}$$

$$d_{h,res} = b_2 d_{h,y} \tag{15}$$

Figure 19 shows an example of the regression analysis for the considered aspect ratios ranging approximately from 1.0 to 1.8. Additional experimental tests and/or numerical simulations would lead to a more extensive database covering a wider range of aspect ratios, material properties, infill thickness, etc., and hence different solutions to the regression analysis could be used. It should be mentioned that a threshold R^2 value equal to 0.8 was adopted for curve fitting, *i.e.* when a linear model was associated with a R^2 lower than the threshold value, a higher-order polynomial model was used until the corresponding R^2 is larger than 0.8. Figure 19a and 19b show the determination of the constant coefficients α and β, which are approximately equal to 0.05 and 0.82, respectively. Figure 19c to 19f present the regression models for the remaining coefficient (a_1, a_2, b_1 and b_2) with respect to the aspect ratio, where each of the regression models achieved a R^2 larger than 0.8, indicating a good curve fitting.

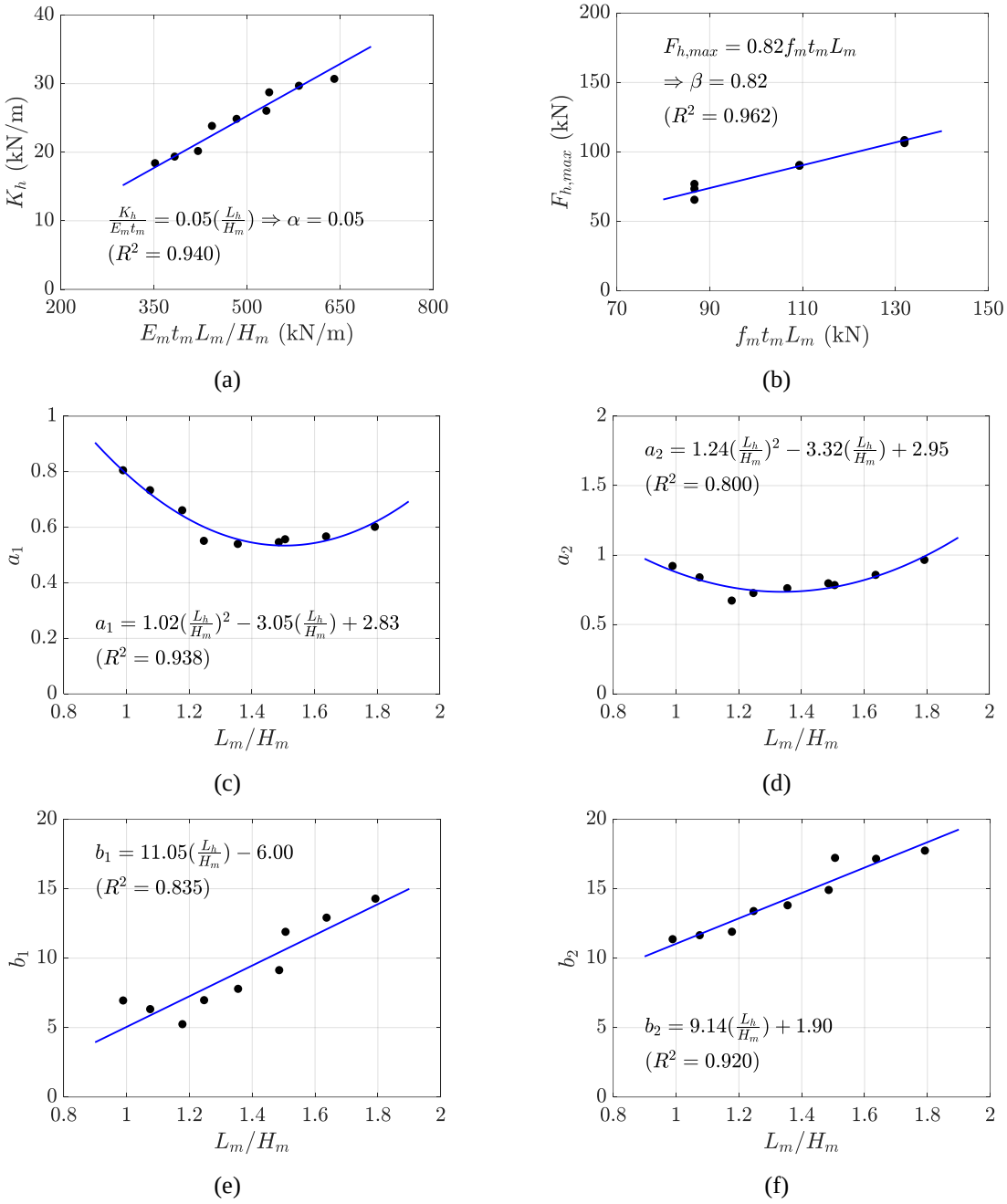

Figure 19. Regression models of the constant coefficients α and β, and coefficients a_1, a_2, b_1 and b_2 with respect to the aspect ratio of infill walls.

4.3 Validation of the single-strut model

In order to validate the force-displacement model developed by the regression analysis, four new FE models of infilled steel frame were built in Abaqus. The geometric characteristics of the four additional models are summarised in Table 8. The four models had different heights, widths and aspect ratios of infill walls compared to those included in the database. Then the corresponding single-strut models were built in OpenSees following the formulation described by Eq.(8) to Eq.(15) and the regression models summarised in Figure 19. The comparisons of global response between the single-strut models and the micro-models are provided in Figure 20. It can be concluded that the comparison shows a good agreement of the results, demonstrating the ability of the adopted methodology in developing non-linear single-strut models for masonry infills.

Table 8. Geometric properties of the FE models used to validate the regression model.

Model	E_{adj} (MPa)	L (mm)	H (mm)	L_{Infill} (mm)	H_{Infill} (mm)	$(L/H)_{Infill}$ (-)
model-V1	6122	2906	2761	2900	2511	1.155
model-V2	6186	2906	2947	2900	2697	1.075
model-V3	6165	3106	2203	3100	1953	1.587
model-V4	6165	3306	2203	3300	1953	1.690

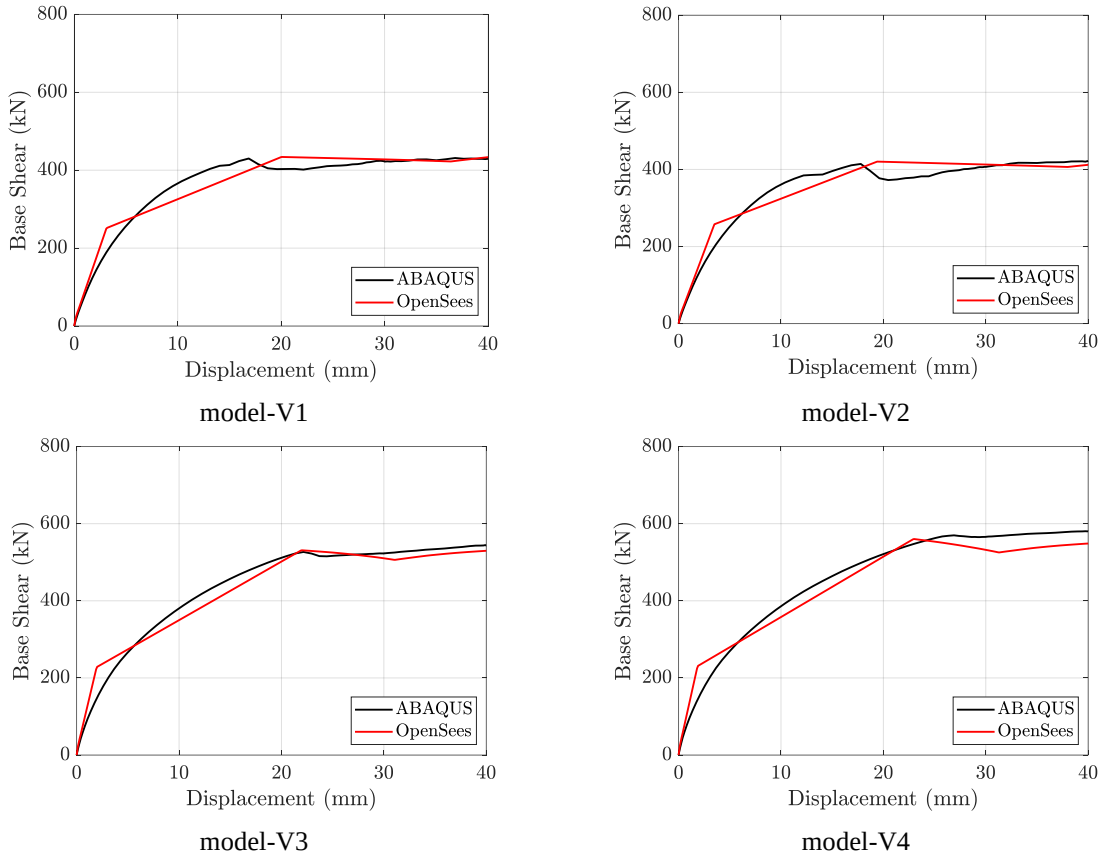

Figure 20. Validation of the regression model by comparing the global responses.

5. CONCLUSIONS

This paper presented a framework for the development of generalised force-displacement relationships for single-strut models for masonry infills walls within existing steel moment-resisting frames (MRFs). A methodology based on a genetic algorithm (GA) optimisation was presented and applied to a database of case study infilled steel MRFs to calibrate the modelling parameters. The framework involves three main steps: firstly, to establish a database of infilled steel frames from experiments and/or advanced numerical simulations; then to calibrate the modelling parameters of masonry strut models; finally, to build regression model of the force-displacement relationship for masonry struts.

The framework was demonstrated in detail through a database of case study infilled steel MRFs developed from FE micro-models validated against experimental results. It was shown that the GA was capable of calibrating the modelling parameters of the single-strut models in an effective and efficient manner, and the implementation of this framework is able to effectively lead to the development of generalised force-displacement relationships of masonry strut models with good accuracy in predicting the global response of infilled structures. Some other conclusions can also be drawn from the case study. It was observed that the aspect ratio (L_m/H_m) have a great impact on the behaviour of infill walls, including the formation of the compressive strut and the damage pattern

occurred inside the compressive strut zone. Thus, such parameter was considered a major aspect defining the seismic response of infilled steel MRFs and was adopted in the formulation of force-displacement relation of the single-strut model. The analysis of the case study also showed that the single-strut models developed and used in this study were not able to properly simulate the local responses (*i.e.*, forces and deformations) in columns, as a consequence of the modelling arrangement of the single-strut within the steel frame, leading to around 80% underestimation of the shear force demand and up to 50% underestimation of the bending moment demand. However, this is a well-known limitation of such a simplified modelling strategy. Conversely, the results showed the ability of the developed models in simulating the global response of the structures.

It is worth highlighting that the regression parameters determined in this study have been derived from a limited database. However, the proposed methodology can be used to incorporate additional data from experimental tests and numerical simulations hence updating the regression parameters and providing more general results. Moreover, it is worth mentioning that machine learning-based regression model, such as support vector machine, Gaussian process regression and artificial neural network, could be more advantageous in some situations, particularly when several parameters are required to be included in the regression analysis at predictors. Further studies should be performed to explore the possibility of machine learning-based methods within the framework of seismic assessment of existing buildings.

ACKNOWLEDGEMENTS

This work was supported by the Seismology and Earthquake Engineering Research Infrastructure Alliance for Europe (SERA) within the H2020-INFRAIA-2016-2017 Framework Programme of the European Commission under grant agreement No. 730900. Any opinions, findings and conclusions, or recommendations expressed in this paper are those of the authors and do not necessarily reflect those of SERA sponsors.

REFERENCES

1. Asteris PG, Antoniou ST, Sophianopoulos DS, Chrysostomou CZ. Mathematical macromodeling of infilled frames: state of the art. *Journal of Structural Engineering*. 2011;137: 1508-1517. https://doi.org/10.1061/(ASCE)ST.1943-541X.0000384
2. Mohammad Noh N, Liberatore L, Mollaioli F, Tesfamariam S. Modelling of masonry infilled RC frames subjected to cyclic loads: State of the art review and modelling with OpenSees. *Engineering Structures*. 2017;150: 599-621. https://doi.org/10.1016/j.engstruct.2017.07.002
3. Di Sarno L, Wu J-R. Fragility assessment of existing low-rise steel moment-resisting frames with masonry infills under mainshock-aftershock earthquake sequences. *Bulletin of Earthquake Engineering*. 2021;19(6): 2483-2504. https://doi.org/10.1007/s10518-021-01080-6
4. Freddi F, Novelli V, Gentile R, Veliu E, Andonov A, Andreev S, Greco F, Zhuleku E. Observations from the 26th November 2019 Albania Earthquake: the Earthquake Engineering Field Investigation Team (EEFIT) mission. *Bulletin of Earthquake Engineering*. 2021;19(5): 2013-2044. https://doi.org/10.1007/s10518-021-01062-8
5. Mpampatsikos V, Nascimbene R, Petrini L. A critical review of the RC frame existing building assessment procedure according to Eurocode 8 and Italian seismic code. *Journal of Earthquake Engineering*. 2008;12(S1): 52-82. https://doi.org/10.1080/13632460801925020
6. Araújo M, Castro JM. A critical review of European and American provisions for the seismic assessment of existing steel moment-resisting frame buildings. *Journal of Earthquake Engineering*. 2018;22(8): 1336-1364. https://doi.org/10.1080/13632469.2016.1277568
7. Gutiérrez-Urzúa F, Freddi F, Di Sarno L. Comparative analysis of code-based approaches for seismic assessment of existing steel moment resisting frames. *Journal of Constructional Steel Research*. 2021;181: 106589. https://doi.org/10.1016/j.jcsr.2021.106589
8. Di Sarno L, Wu J-R. Seismic assessment of existing steel frames with masonry infills. *Journal of Constructional Steel Research*. 2020;169: 106040. https://doi.org/10.1016/j.jcsr.2020.106040
9. Smith BS. Lateral stiffness of infilled frames. *Journal of the Structural Division*. 1962;88(6): 183-199. https://doi.org/10.1061/JSDEAG.0000849

10. Stafford Smith B, Carter C. A method of analysis for infilled frames. *Proceedings of the institution of civil engineers.* 1969;44(1): 31-48. https://doi.org/10.1680/iicep.1969.7290

11. Mainstone RJ. *Supplementary note on the stiffness and strengths of infilled frames*. Watford: Building Research Establishment; 1974.

12. Moghaddam HA. Lateral load behavior of masonry infilled steel frames with repair and retrofit. *Journal of Structural Engineering*. 2004;130(1): 56-63. https://doi.org/10.1061/(ASCE)0733-9445(2004)130:1(56)

13. Chen X, Liu Y. Numerical study of in-plane behaviour and strength of concrete masonry infills with openings. *Engineering Structures*. 2015;82: 226-235. https://doi.org/10.1016/j.engstruct.2014.10.042

14. Asteris PG, Cavaleri L, Di Trapani F, Tsaris AK. Numerical modelling of out-of-plane response of infilled frames: State of the art and future challenges for the equivalent strut macromodels. *Engineering Structures*. 2017;132: 110-122. https://doi.org/10.1016/j.engstruct.2016.10.012

15. Mehrabi AB, Shing PB, Schuller M, and Noland J. Experimental evaluation of masonry-infilled RC frames. *Journal of Structural Engineering*. 1996;122(3): 228-237. https://doi.org/10.1061/(ASCE)0733-9445(1996)122:3(228)

16. Buonopane SG, White RN. Pseudodynamic testing of masonry infilled reinforced concrete frame. *Journal of Structural Engineering*. 1999;125(6): 578-589. https://doi.org/10.1061/(ASCE)0733-9445(1999)125:6(578)

17. Žarnić R, Gostič S, Crewe AJ, Taylor CA. Shaking table tests of 1:4 reduced-scale models of masonry infilled reinforced concrete frame buildings. *Earthquake Engineering and Structural Dynamics*. 2001;30(6); 819-834. https://doi.org/10.1002/eqe.39

18. Hashemi A, Mosalam KM. Shake-table experiment on reinforced concrete structure containing masonry infill wall. *Earthquake Engineering and Structural Dynamics*. 2006;35(14): 1827-1852. https://doi.org/10.1002/eqe.612

19. Asteris PG, Repapis CC, Repapi EV, Cavaleri L. Fundamental period of infilled reinforced concrete frame structures. *Structure and Infrastructure Engineering*. 2017;13(7): 929-941. https://doi.org/10.1080/15732479.2016.1227341

20. Moghadam HA, Mohammadi MG, Ghaemian M. Experimental and analytical investigation into crack strength determination of infilled steel frames. *Journal of Constructional Steel Research*. 2006;62(12): 1341-1352. https://doi.org/10.1016/j.jcsr.2006.01.002

21. Ghazimahalleh MM. Stiffness and damping of infilled steel frames. *Proceedings of the Institution of Civil Engineers-Structures and Buildings*. 2007;160(2): 105-118. https://doi.org/10.1680/stbu.2007.160.2.105

22. Tasnimi AA, Mohebkhah A. Investigation on the behavior of brick-infilled steel frames with openings, experimental and analytical approaches. *Engineering Structures*. 2011;33(3): 968-980. https://doi.org/10.1016/j.engstruct.2010.12.018

23. Liu Y, Manesh P. Concrete masonry infilled steel frames subjected to combined in-plane lateral and axial loading - An experimental study. *Engineering Structures*. 2013;52: 331-339. https://doi.org/10.1016/j.engstruct.2013.02.038

24. Markulak D, Radić I, Sigmund V. Cyclic testing of single bay steel frames with various types of masonry infill. *Engineering structures*. 2013;51: 267-277. https://doi.org/10.1016/j.engstruct.2013.01.026

25. Najarkolaie KF, Mohammadi M, Fanaie N. Realistic behavior of infilled steel frames in seismic events: experimental and analytical study. *Bulletin of Earthquake Engineering*. 2017;15(12): 5365-5392. https://doi.org/10.1007/s10518-017-0173-z

26. Di Sarno L, Freddi F, D'Aniello M, Kwon OS, Wu JR, Gutiérrez-Urzúa F, Landolfo R, Park J, Palios X, Strepelias E. Assessment of existing steel frames: Numerical study, pseudo-dynamic testing and influence of masonry infills. *Journal of Constructional Steel Research*. 2021;185: 106873. https://doi.org/10.1016/j.jcsr.2021.106873

27. Fardis MN, Panagiotakos TB. Seismic design and response of bare and masonry-infilled reinforced concrete buildings part II: infilled structures. Journal of Earthquake Engineering. 1997;1(03): 475-503. https://doi.org/10.1080/13632469708962375

28. Dolšek M, Fajfar P. The effect of masonry infills on the seismic response of a four-storey reinforced concrete frame - a deterministic assessment. *Engineering Structures*. 2008;30(7): 1991-2001. https://doi.org/10.1016/j.engstruct.2008.01.001

29. Liberatore L, Decanini LD. Effect of infills on the seismic response of high-rise RC buildings designed as bare according to Eurocode 8. *Ingegneria sismica*. 2011;28(3): 7-23.

30. El-Dakhakhni WW, Elgaaly M, Hamid AA. Three-strut model for concrete masonry-infilled steel frames. *Journal of Structural Engineering*. 2003;129(2): 177-185. https://doi.org/10.1061/(ASCE)0733-9445(2003)129:2(177)

31. Yekrangnia M, Mohammadi M. A new strut model for solid masonry infills in steel frames. *Engineering Structures*. 2017;135: 222-235. https://doi.org/10.1016/j.engstruct.2016.10.048

32. Pashaie MR, Mohammadi M. An extended multiple-strut model to estimate infill effects on multi-storey steel frames with different connection rigidities. *Structures* 2021;30: 710-734. https://doi.org/10.1016/j.istruc.2020.12.035

33. Goldberg DE, Holland JH. Genetic algorithms and machine learning. *Machine Learning*. 1988;3(2): 95-99. https://doi.org/10.1023/A:1022602019183

34. Lipowski A, Lipowska D. Roulette-wheel selection via stochastic acceptance. *Physica A: Statistical Mechanics and its Applications*. 2012;391(6): 2193-2196. https://doi.org/10.1016/j.physa.2011.12.004

35. Dassault Systèmes. ABAQUS/Standard User's Guide, Version 6.14. Providence: Dassault Systèmes Simulia Corporation; 2014.

36. Abdulla KF, Cunningham LS, Gillie M. Simulating masonry wall behaviour using a simplified micro-model approach. *Engineering Structures*. 2017;151: 349-365. https://doi.org/10.1016/j.engstruct.2017.08.021

37. Dhir P.K., Tubaldi E., Ahmadi H., Gough J. Numerical modelling of reinforced concrete frames with masonry infills and rubber joints. *Engineering Structures*. 2021;246: 112833. https://doi.org/10.1016/j.engstruct.2021.112833

38. da Porto F, Guidi G, Garbin E, Modena C. In-plane behavior of clay masonry walls: experimental testing and finite-element modeling. *Journal of structural engineering*. 2010;136(11): 1379-1392. https://doi.org/10.1061/(ASCE)ST.1943-541X.0000236

39. Benzeggagh ML, Kenane MJ. Measurement of mixed-mode delamination fracture toughness of unidirectional glass/epoxy composites with mixed-mode bending apparatus. *Composites science and technology*. 1996;56(4): 439-449. https://doi.org/10.1016/0266-3538(96)00005-X

40. Lourenço PJ. *Computational strategies for masonry structures* [PhD thesis]. Delft: Delft University Press; 1996.

41. Campione G, Cavaleri L, Macaluso G, Amato G, Di Trapani F. Evaluation of infilled frames: an updated in-plane-stiffness macro-model considering the effects of vertical loads. *Bulletin of Earthquake Engineering*. 2015;13(8): 2265-2281. https://doi.org/10.1007/s10518-014-9714-x

42. European Committee for Standarization. Eurocode 3. *Design of steel structures. General rules and rules for buildings*. London: British Standard Institution; 2005.

43. Mazzoni S, McKenna F, Scott MH, Fenves GL. OpenSees command language manual. *Pacific Earthquake Engineering Research (PEER) Center*. 2006;264: 137-158.

44. Lignos DG, Krawinkler H. Deterioration modelling of steel components in support of collapse prediction of steel moment frames under earthquake loading. *Journal of Structural Engineering*. 2011;137(11): 1291-1302. https://doi.org/10.1061/(ASCE)ST.1943-541X.0000376

45. Zareian F, Medina RA. A practical method for proper modelling of structural damping in inelastic plane structural systems. *Computers and Structures*. 2010;88(1–2): 45-53. https://doi.org/10.1016/j.compstruc.2009.08.001